Supporting Information

Meta-Linkage Strategy Towards High-Performance Hosts for Efficient Blue Thermally Activated Delayed Fluorescence OLEDs

Xiao-Dong Tao,[a,b,d] Zhuangzhuang Wei,[a,d,e] Lingyi Meng,[a,d,e] Xu-Lin Chen,[*a,c,d] Mingxue Yang,[a,d] Yan-Yun Jing,[a,b] Dong-Hai Zhang,[a,b,d] and Can-Zhong Lu [*a,b,c,d]

[a] CAS Key Laboratory of Design and Assembly of Functional Nanostructures, Fujian Provincial Key Laboratory of Nanomaterials, Fujian Institute of Research on the Structure of Matter, Chinese Academy of Sciences, Fuzhou, Fujian 350002, China. E-mail: czlu@fjirsm.ac.cn (C. Z. Lu), xlchem@fjirsm.ac.cn (X. L. Chen).

[b] University of Chinese Academy of Sciences, Beijing 100049, China.

[c] Fujian Science & Technology Innovation Laboratory for Optoelectronic Information of China, Fuzhou, Fujian 350108, P. R. China.

[d] Xiamen Key Laboratory of Rare Earth Photoelectric Functional Materials, Xiamen Institute of Rare Earth Materials, Haixi Institutes, Chinese Academy of Sciences, Xiamen, Fujian 361021, P. R. China.

[e] College of Chemistry and Materials Science, Fujian Normal University, Fuzhou City, Fujian Province 350007, P. R. China.

Contents

1. Materials and instruments (General information)

^{1}H NMR and ^{13}C NMR spectra were recorded on a Bruker Avance III 500 MHz NMR spectrometer. Elemental analyses (C, H, O) were performed on an Elementary Vario EL III element analyzer. Diffraction data were collected on a D8 VENTRUE diffractometer equipped with Mo K_{α} radiation (λ = 0. 7093 Å) at 200 K. The crystal structure was solved by direct method and difference fourier syntheses. Thermogravimetric analysis (TGA) and differential scanning calorimetry (DSC) were performed by Mettler-Toledo TGA/DSC 1. The test was under nitrogen atmosphere at the heating rate of 20 °C/min. Cyclic voltammetric (CV) were performed on a CHI840D Electrochemical Analyzer with scanning rate of 100 mV/s at room temperature, using a glassy carbon working electrode, a platinum wire auxiliary electrode, and a silver/silver nitrate ($Ag/AgNO_3$) reference electrode. The film morphologies were measured by using a Bruker Dimension ICON atomic force microscope. The UV-visible absorption spectra were measured using Agilent Cary 5000 UV-vis spectrophotometer at room temperature. Steady-state PL spectra were measured on Edinburgh FLS980 using a xenon lamp as an excitation light source. The transient PL decay curves were measured on the same spectrophotometer (FLS980) in time-correlated single-photon counting mode with an NT242-1K OPO laser as a light source. The time-resolved PL spectra were recorded on an Edinburgh LP980 spectrophotometer with an NT242-1K OPO laser excitation source. The absolute photoluminescence quantum yields were measured by a HORIBA Jobin-Yvon FluoroMax-4 spectrometer equipped with an integrating sphere.

2. Synthesis

Synthesis of tris(4-(diphenylphosphanyl oxide)phenyl)phosphane oxide (p4PO)

The tris(4-(diphenylphosphanyl oxide)phenyl)phosphane oxide was synthesized according to previous reports.[1]

Synthesis of tris(3-(diphenylphosphanyl oxide)phenyl)phosphane oxide (m4PO)

To a solution of triphenylphosphine (5.25 g, 20 mmol) in 40 ml dry THF in a 250 ml two-necked round-bottom flask, fresh-cut sodium pieces (1.84 g, 80 mmol) was added under N_2 atmosphere. The mixture was stirred at 80 ℃ for 12 h. After cooling to room temperature, the reaction solution was added dropwise into a solution of tris(3-fluorophenyl)phosphine (1.896 g , 6 mmol) in THF (12 ml) under N_2 atmosphere and stirred at room temperature for 1 hour, then heated to reflux and stirred overnight. After removing the solvents, the residue was dissolved in dichloromethane, to which added H_2O_2 (30 %, 30 ml) slowly and stirred for 4 h at room temperature. The reaction mixture was extracted three times with CH_2Cl_2. The combined extracts were dried over anhydrous Na_2SO_4, filtered and concentrated under reduced pressure. The residue was purified on silica gel to afford the target compound m4PO (3.27 g, yield: 62 %). ^{1}H NMR (500 MHz, Chloroform-d) δ 7.90 - 7.84 (m, 3H), 7.77 (t, J = 11.7 Hz, 3H), 7.69 - 7.61 (m, 3H), 7.58 - 7.45 (m, 21H), 7.39 (t, J = 7.6 Hz, 12H). ^{13}C NMR (101 MHz, Chloroform-d) δ 135.93, 135.86, 135.25, 135.15, 135.04, 134.69, 134.58, 133.69, 133.58, 132.66, 132.55, 132.34, 132.31, 131.98, 131.94, 131.88, 131.63, 131.52, 130.90, 129.08, 128.97, 128.85, 128.79, 128.67. ^{31}P NMR (162 MHz, Chloroform-d): δ 28.19, 28.18, 26.90, 26.88. MS (m/z): $[M+Na]^+$ Calcd. for $C_{54}H_{42}P_4O_4Na$, 901.79; found, 901.1926. Anal. Calcd. for $C_{54}H_{42}P_4O_4$: C, 73.80, H, 4.88. Found: C, 73.60, H, 4.94.

Synthesis of tris(3-(carbazole)phenyl)phosphane oxide (m3CzPO)

A solution of (3-bromophenyl)carbazole (6.64 g, 20 mmol) in 40 mL dry THF was cooled under a nitrogen atmosphere down to -78 ℃. A solution of n-butyllithium (2.5 M, 22 mmol, 8.8 mL) was slowly added into the mixture under the -78 ℃ and stirred for 3 h. Then phosphorus(III) chloride (0.822 g, 6 mmol) was added into the mixture.

The resulting mixture was gradually warmed to ambient temperature and stirred for 8 h. The reaction mixture was quenched with methanol, and then the solvent was evaporated under reduced pressure. The residue was dissolved in dichloromethane, to which H_2O_2 (30 %, 30 ml) was added slowly. After stirring for 4 h at room temperature, the reaction mixture was extracted three times with dichloromethane. The combined extracts were dried over anhydrous Na_2SO_4, filtered and concentrated under reduced pressure. The residue was purified by column chromatography on silica gel to afford m3CzPO as a white solid (2.23 g, yield: 48 %). ^{1}H NMR (500 MHz, Chloroform-d): δ 8.09 (d, *J* = 8.1 Hz, 6H), 7.97 (t, *J* = 10.1 Hz, 6H), 7.83 - 7.74 (m, 6H), 7.24 (dd, *J* = 7.2, 6.2 Hz, 12H), 7.21 - 7.16 (m, 6H). ^{13}C NMR (101 MHz, Chloroform-d): δ 140.36, 138.61, 138.49, 134.65, 133.83, 130.98, 130.96, 130.79, 130.76, 130.69, 130.19, 130.10, 126.22, 123.61, 120.48, 120.40, 109.35. MS (m/z): $[M+Na]^+$ Calcd. for $C_{54}H_{36}N_3PONa$, 796.85; found, 796.2488. Anal. Calcd. for $C_{54}H_{36}N_3PO$: C, 83.81, H, 4.69, N, 5.43. Found: C, 84.10, H, 4.73, N, 5.48.

3. Single crystal data

Table S1. Single crystal data of **m3CzPO**

Empirical formula	$C_{54}H_{36}N_3OP$	
CCDC number	2117193	
Formula weight	773.83	
Temperature/K	200.0	
Crystal system	Monoclinic	
Space group	$P2_1/n$	
Unit cell parameters	a =16.6720(10) Å	α = 90 °
	b =27.2792(18) Å	β =108.170(3)°
	c =18.3987(11) Å	γ = 90°
Volume/Å^3	7950.5(9) Å^3	
Z	8	
ρ_{calc}	1.293 g/cm^3	
μ	0.115 mm^{-1}	
F(000)	3232.0	
Crystal size	0.3 × 0.2 × 0.2 mm^3	
Radiation	MoKα (λ = 0.71073)	
2Θ range for data collection	3.94 to 55.81 °	
Index ranges	-21 ≤ h ≤ 21, -35 ≤ k ≤ 35, -24 ≤ l ≤ 24	
Reflections collected	119951	
Independent reflections	18826 [R_{int} = 0.2052, R_{sigma} = 0.1269]	
Data/restraints/parameters	18826/0/1063	
Goodness-of-fit on F^2	1.023	
Final R indexes [I>=2σ (I)]	R_1 = 0.0643, wR_2 = 0.1184	
Final R indexes [all data]	R_1 = 0.1739, wR_2 = 0.1633	
Largest diff. peak/hole	0.25/-0.37 e Å^{-3}	

4. TGA&DSC

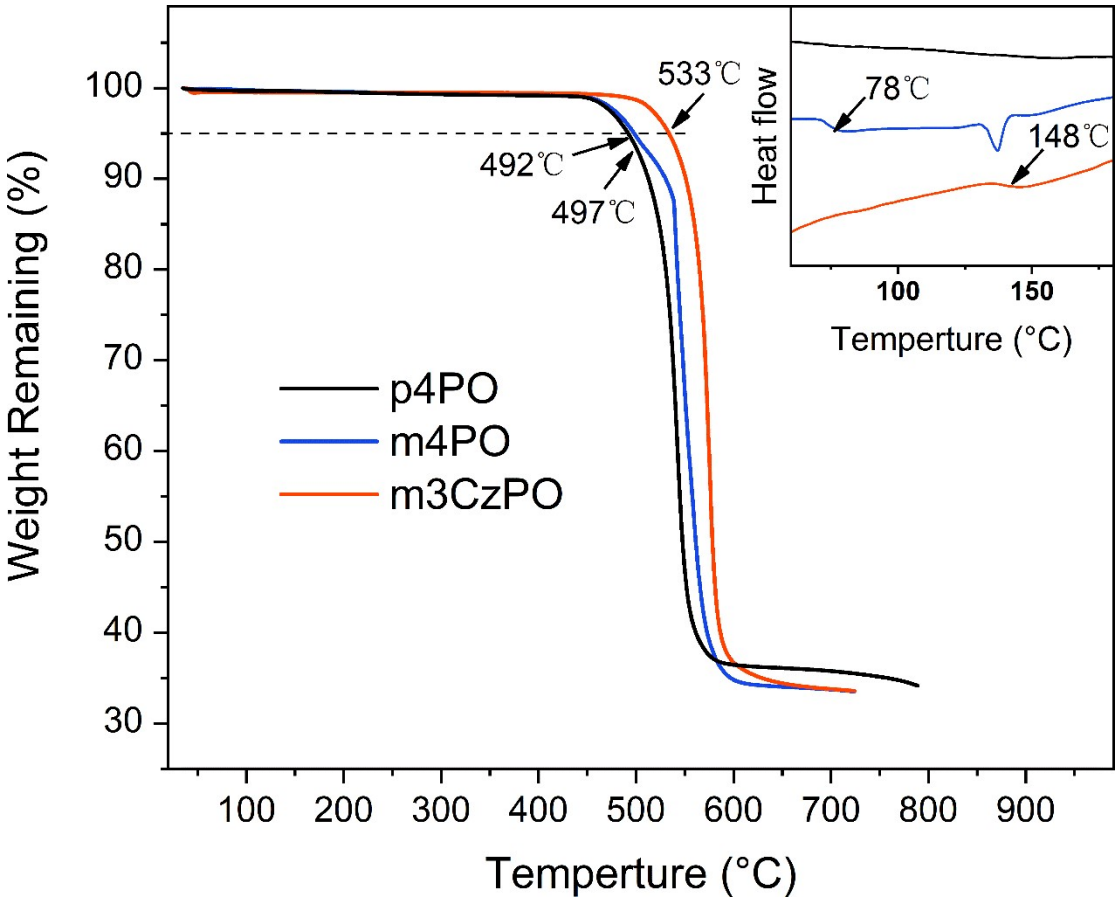

Figure S1. TGA and DSC plots of **p4PO**, **m4PO** and **m3CzPO**. The black dashed line marks 95 % of the original sample weight.

5. AFM

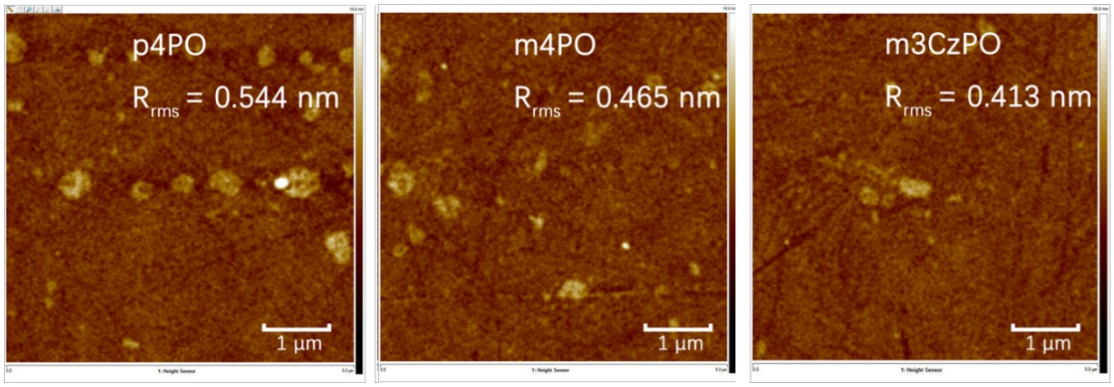

Figure S2. AFM images of vacuum-deposited neat films of **p4PO**, **m4PO** and **m3CzPO**.

6. CV

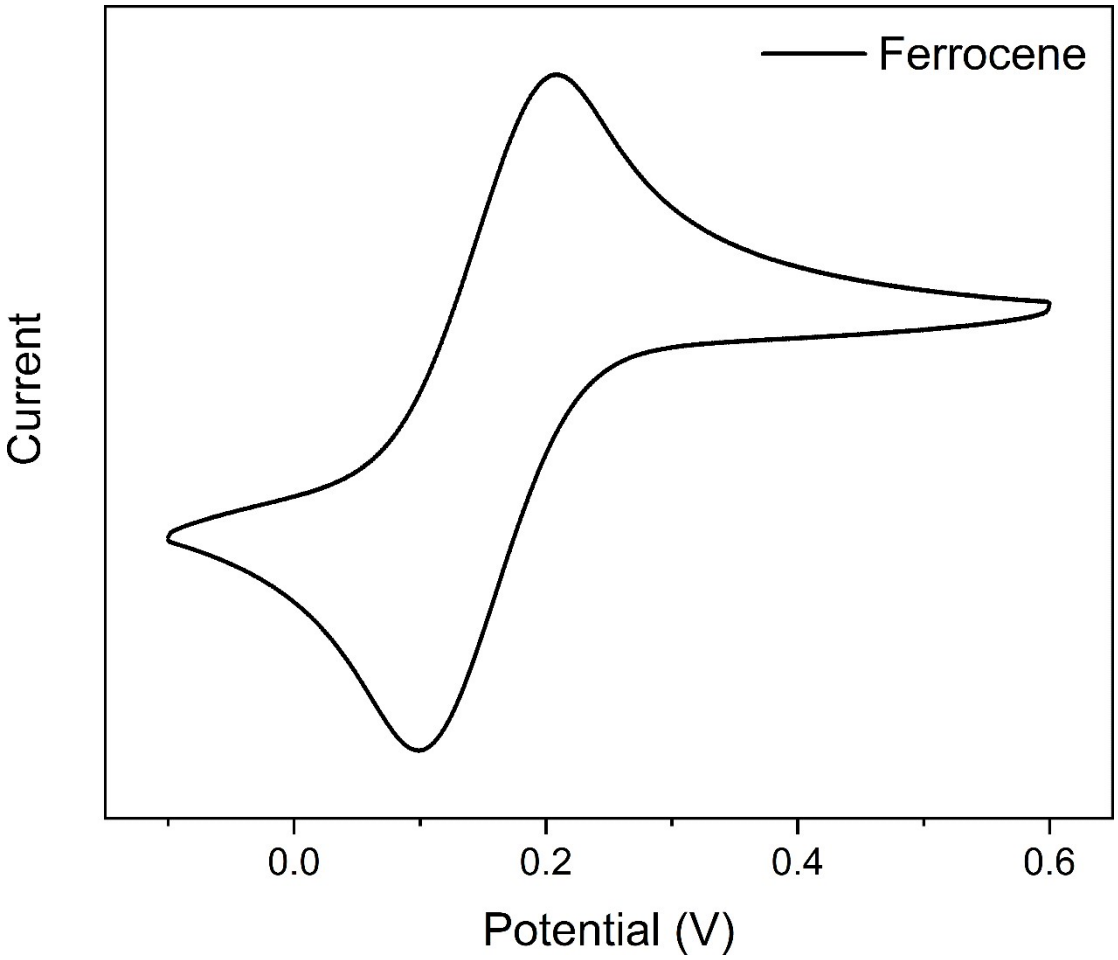

Figure S3. Cyclic voltammograms for the Ferrocene.

HOMO = - [E_{ox} - E(Fc/Fc+) + 4.78] eV

LUMO = - [E_{red} + E(Fc/Fc+) + 4.78] eV

By using the above formulas, HOMO/LUMO levels of p4PO, m4PO and m3CzPO were calculated.

7. Optical properties

Table S2. The photophysical properties of vacuum-evaporated 30 wt% DMAC-DPS doped films using the investigated compounds as host.

host	λ_{em} [a] [nm]	FWHM [b] [nm]	Φ_{PL} [c] [%]	Φ_{PF} / Φ_{DF} [d] [%]	τ_{PF} / τ_{DP} [e] [ns / μs]
p4PO	475	94	86	33/51	18.6/4.19
m4PO	473	91	88	34/54	17.9/3.53
m3CzPO	473	88	89	40/49	18.4/2.53

[a] The emission peak; [b] full width at half maximum; [c] photoluminescence quantum yields; [d] quantum yields of prompt fluorescence (τ_{PF}) and delayed fluorescence (τ_{DF}); [e] prompt fluorescence lifetime and delayed fluorescence lifetime.

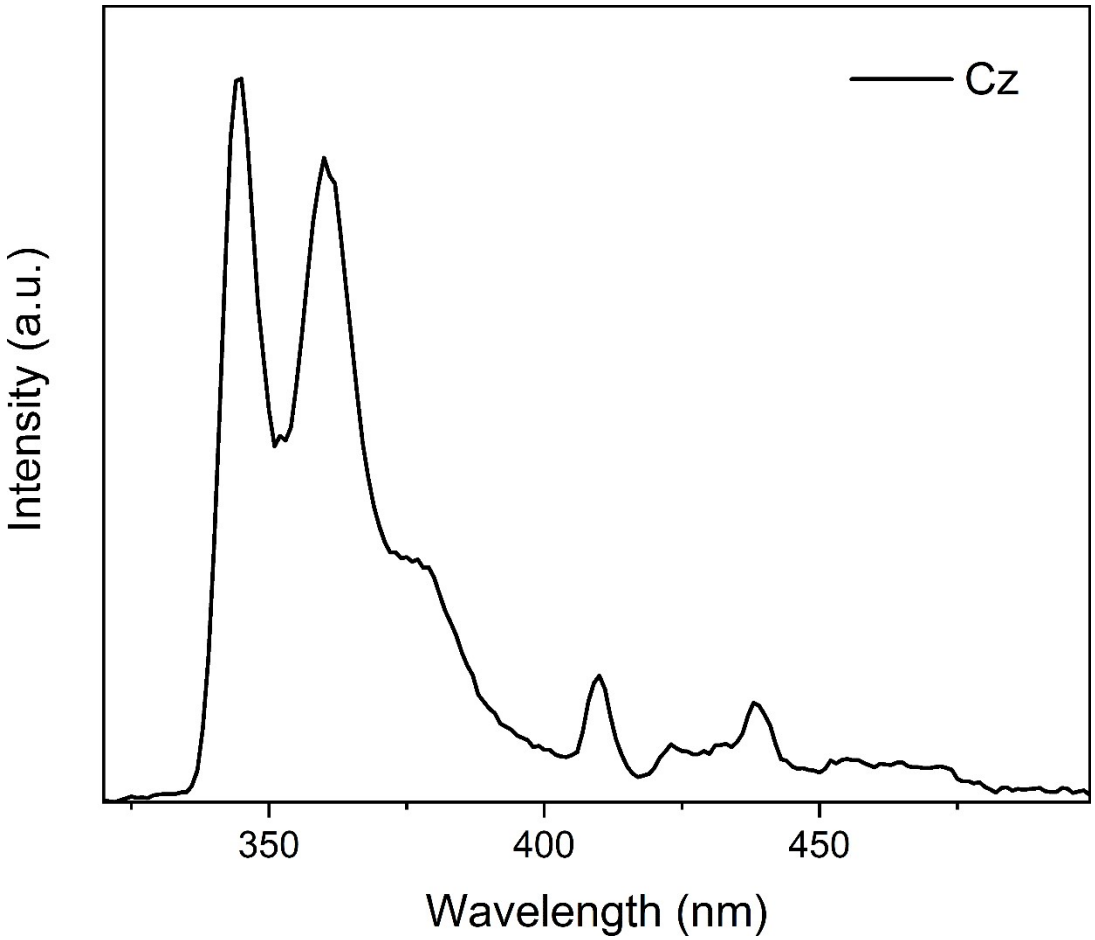

Figure S4. Steady-state photoluminescence spectra of carbazole in 2-MeTHF 1.0 × 10^{-6} M) at 77 K.

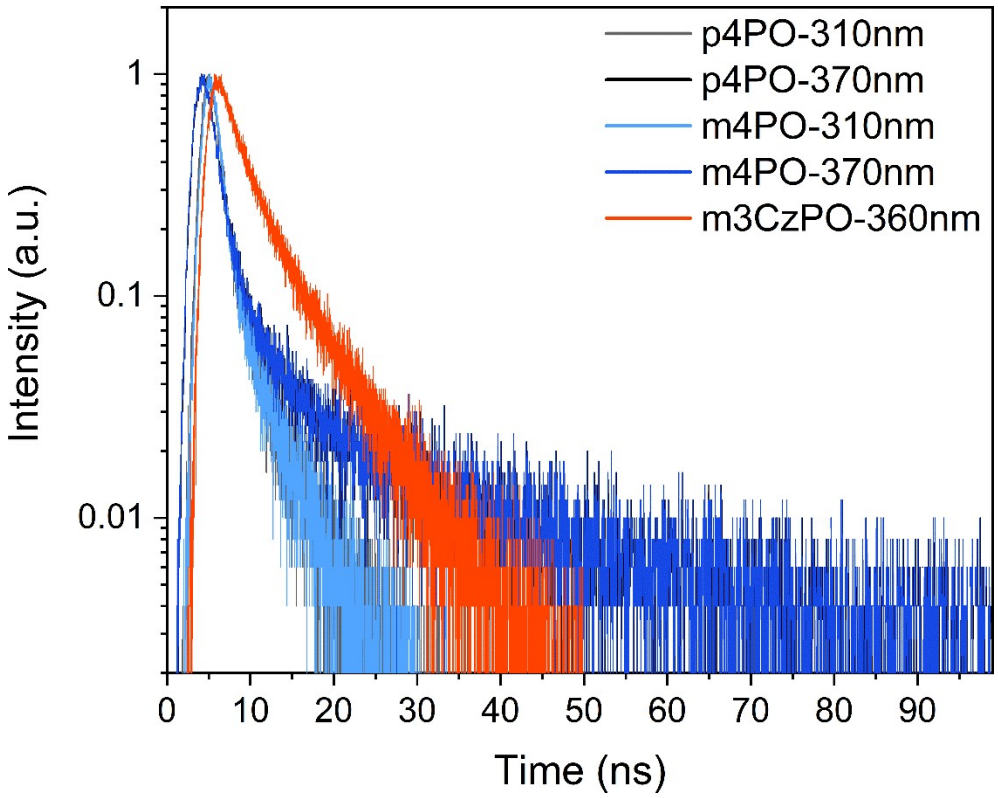

Figure S5. Fluorescence decay of **p4PO**, **m4PO** and **m3CzPO** in 2-MeTHF (1.0×10^{-6} M) at 77 K.

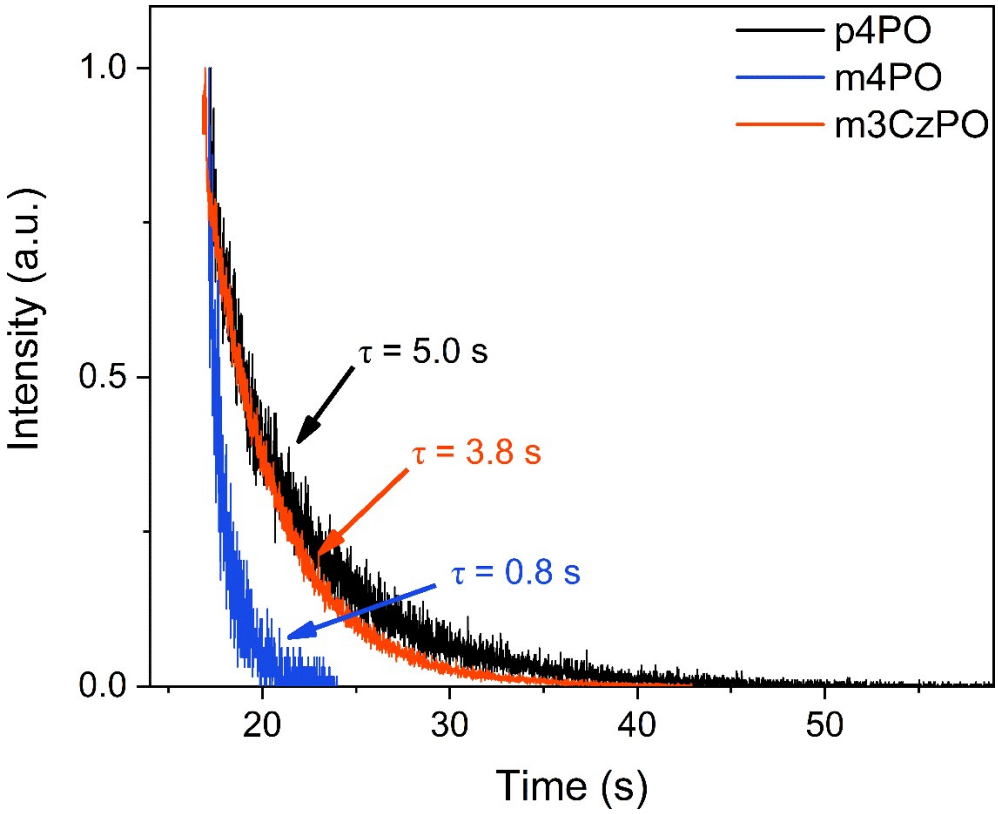

Figure S6. Phosphorescence decay of **p4PO**, **m4PO** and **m3CzPO** in 2-MeTHF (1.0×10^{-6} M) at 77 K.

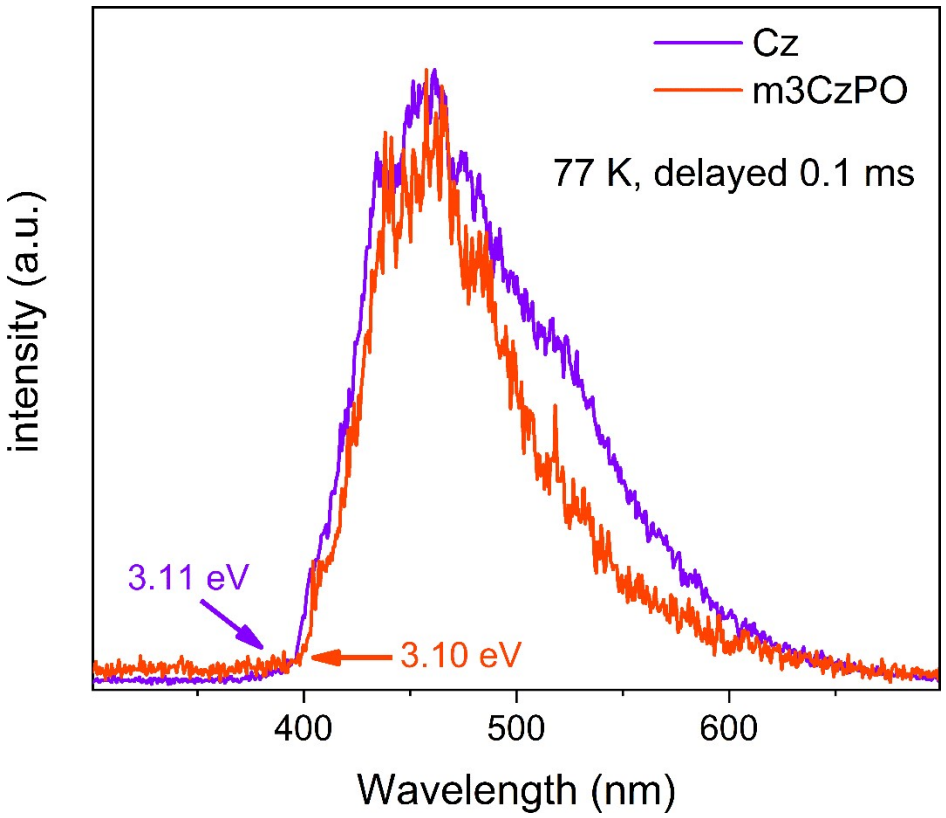

Figure S7. Time-resolved phosphorescence spectra (delayed 0.1 ms) in 2-MeTHF (1.0×10^{-6} M) at 77 K**.**

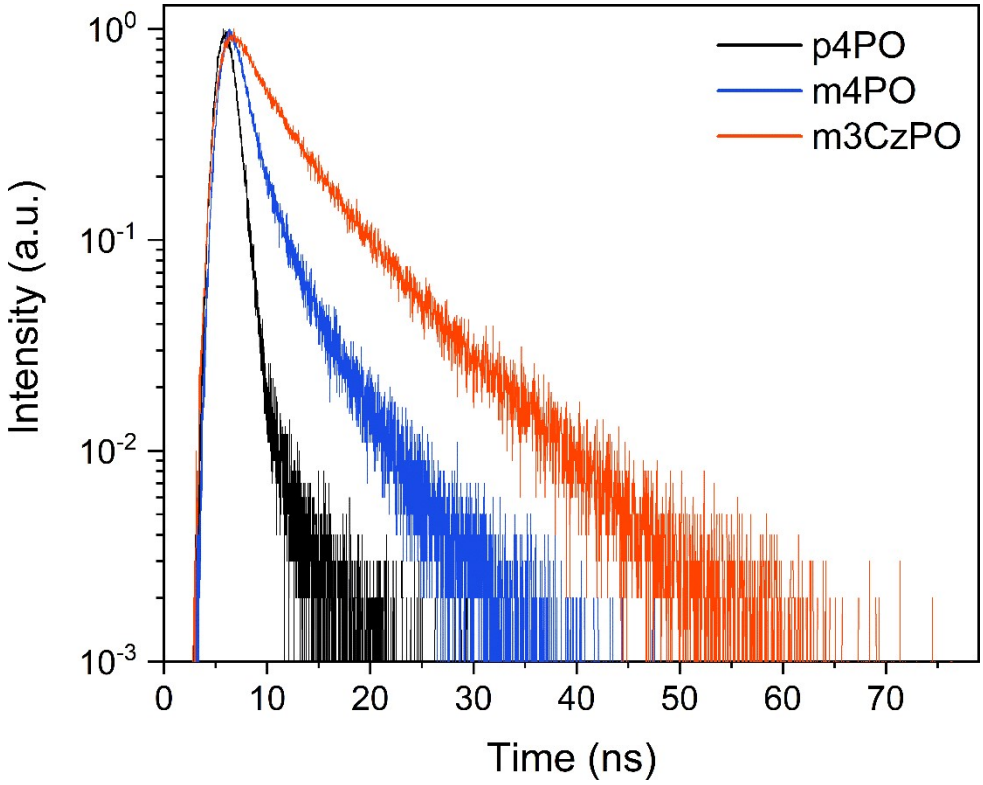

Figure S8. Transient PL decay of p4PO (364 nm), m4PO (370 nm) and m3CzPO (400 nm) in dichloromethane (1.0×10^{-6} M) at room temperature.

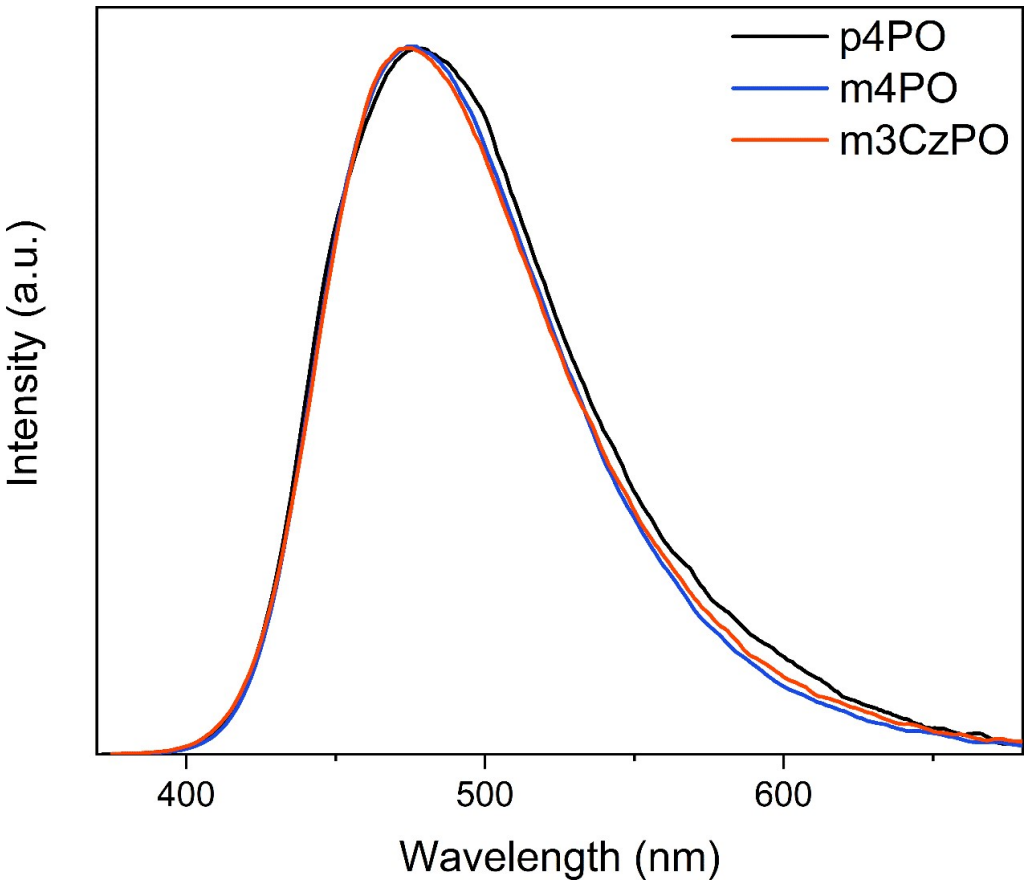

Figure S9. Steady-state photoluminescence spectra of DMAC-DPS-doped films (30 %, 60 nm) using the investigated compounds as hosts (300 K, λ_{ex} =360 nm).

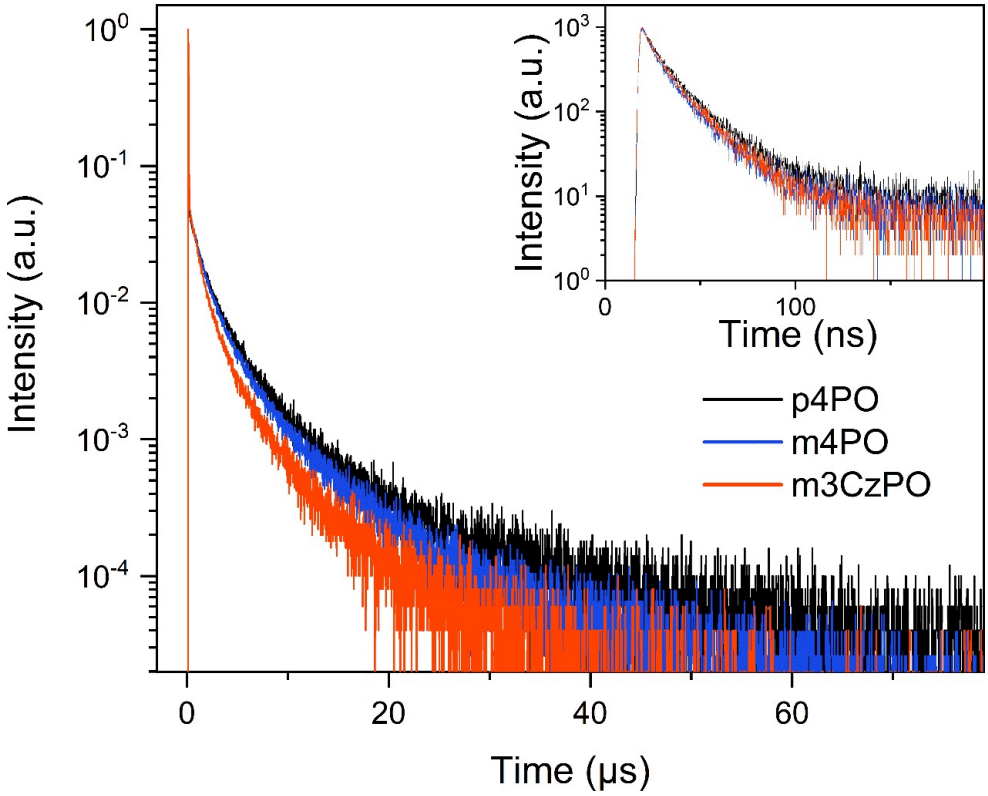

Figure S10. Transient PL decay curves of DMAC-DPS-doped films (30 wt%, 60 nm) using the investigated compounds as hosts (300 K).

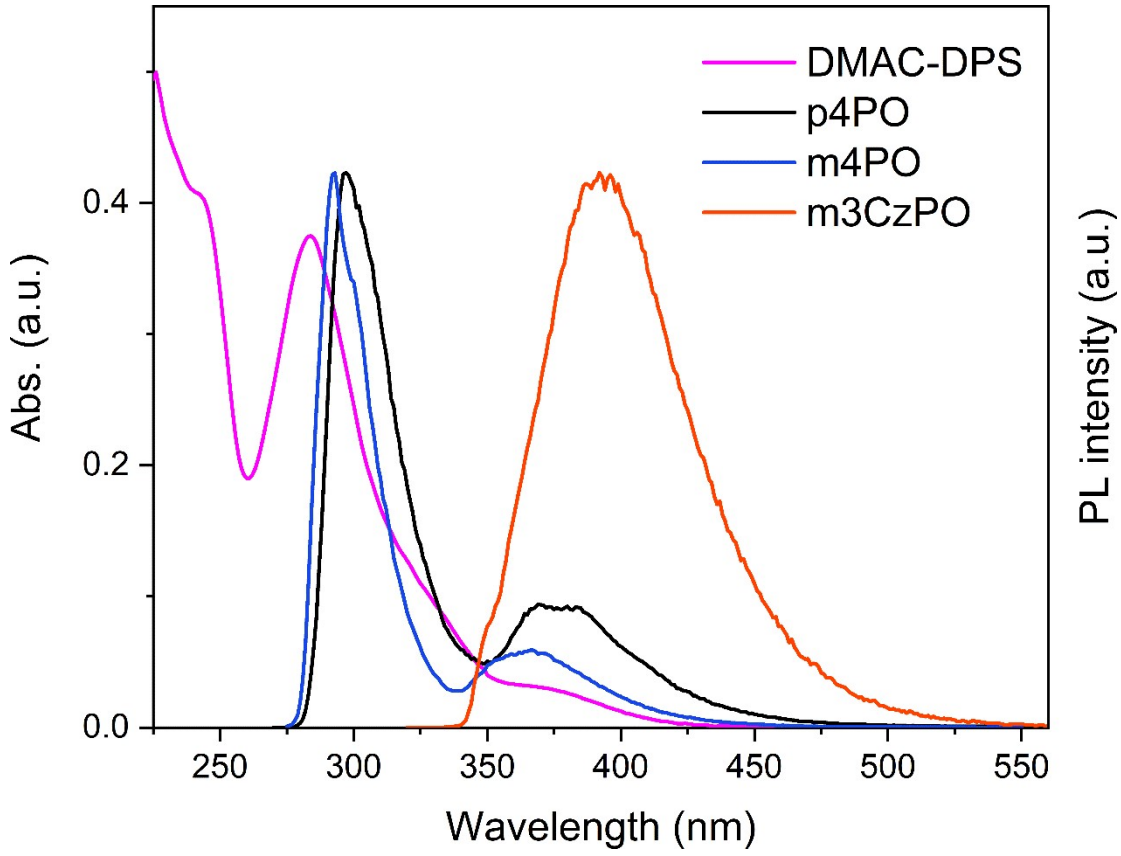

Figure S11. Absorption spectra of DMAC-DPS and photoluminescence spectra of hosts recorded in dichloromethane (1.0×10^{-6} M) at room temperature.

8. OLED fabrication

All organic compounds were purified by temperature-gradient sublimation under high vacuum before use. The thickness and square resistance of ITO were 120 nm and 15 Ω/m^2, respectively. Before fabrication, the ITO substrate was cleaned by detergents and water, and cleaned in the deionized water, acetone and isopropanol for 15 min each in an ultrasonic bath, then stored in absolute ethanol. After being flushed by argon, the ITO glass substrates were treated with UV ozone for 15 min. The organic layer deposition progress was under 2×10^{-5} Pa. The inorganic layer deposition progress was under 4×10^{-4} Pa. The electroluminescence (EL) spectra, *Commission Internatinale de L'Eclairage* coordinates (CIE), current density-voltage (J-V) curves and luminance-voltage (L-V) curves of the devices were measured using a TOPCON SR-UL1R spectroradiometer and Keithley 2400 source meter.

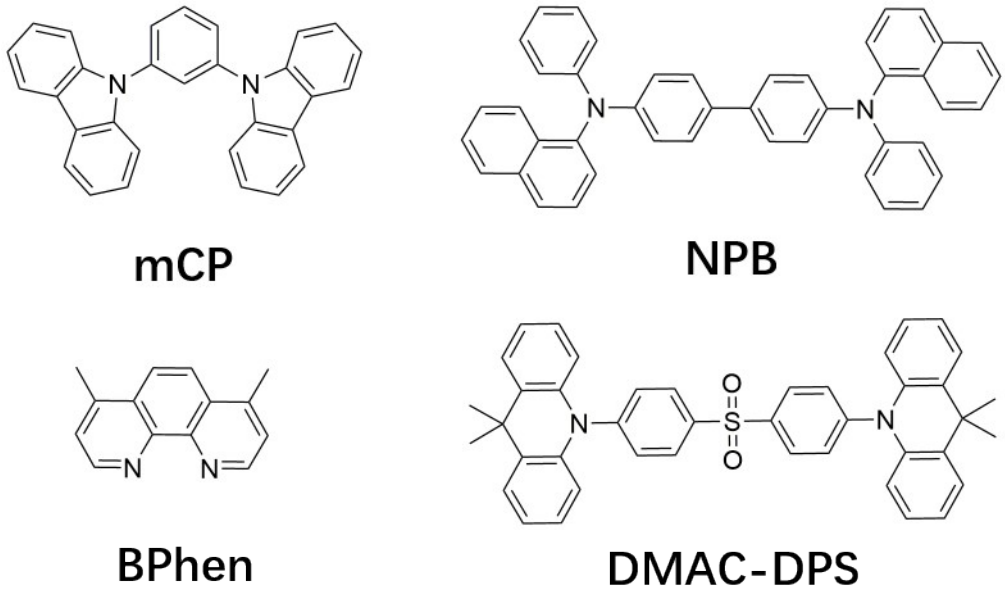

Figure S12. Molecular structures of the functional materials used in the OLEDs.

9. DFT calculations

All the calculations were performed using the Gaussian 09 program package.[2] The density functional theory (DFT) calculations at the PBE/6-311G (d, p) level were performed on the ground state geometries of the investigated compounds using the PBE/6-311G(d, p) level. Time-dependent density functional theory (TD-DFT) calculations were performed at the same level using the optimized ground state geometries. The spin-orbit couplings were calculated at PBE0/DKH by ORCA. Visualizations of the optimized structures and Frontier molecular orbitals was generated using GaussView program and supported to analyze the partition orbital composition by using the Multiwfn 2.4 program.[3]

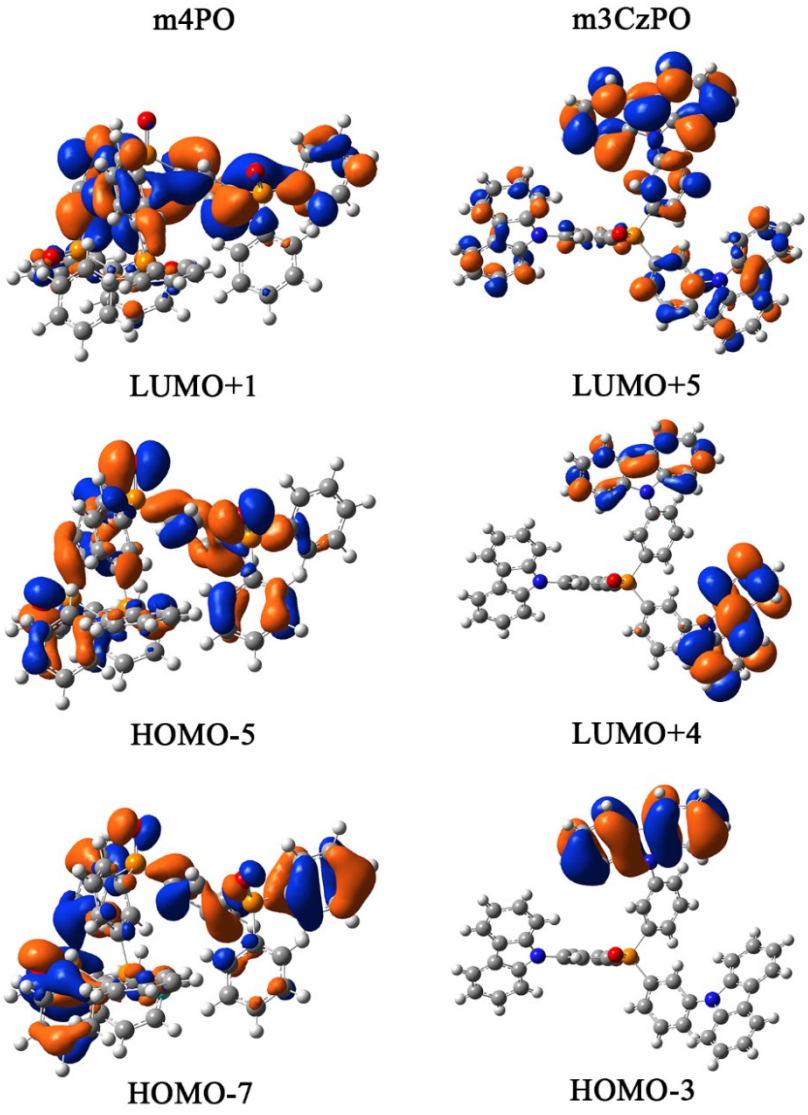

Figure S13. Select molecular orbital distributions of **m4PO** and **m3CzPO**.

Table S3. The lowest vertical energy transitions for **m4PO** and **m3CzPO** determined from TD-DFT calculations.

Molecular	Electronic transitions	E [eV]	Main configurations			
m4PO	S1	4.82	HOMO	→	LUMO	(71.6 %)
m4PO	T1	3.60	HOMO-5	→	LUMO	(6.8 %)
			HOMO-7	→	LUMO+1	(5.7 %)
m3CzPO	S1	3.58	HOMO	→	LUMO	(92 %)
m3CzPO	T1	3.16	HOMO-3	→	LUMO+5	(41.6 %)
			HOMO-3	→	LUMO+4	(13.7 %)

10. Single carrier transporting

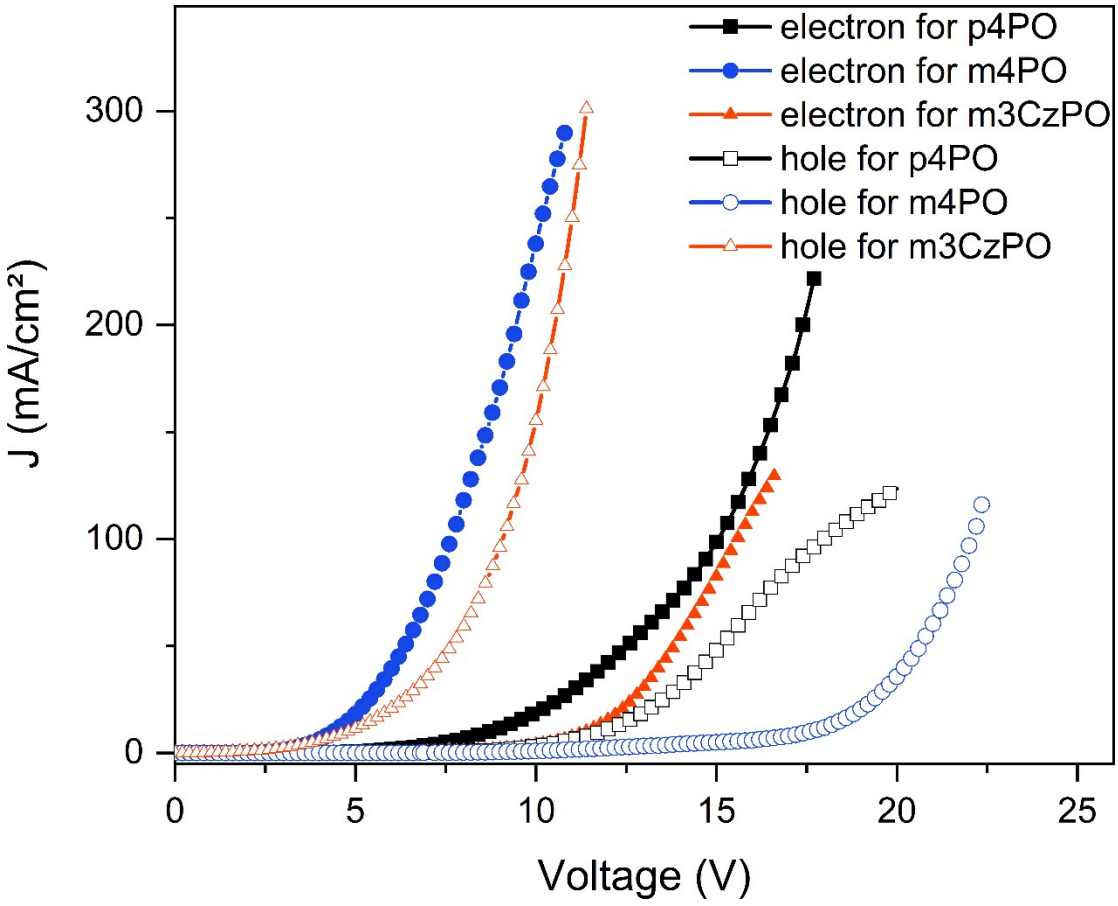

Figure S14. The current density-voltage curves of HOD & EOD based on **p4PO**, **m4PO** and **m3CzPO**.

11. NMR spectra

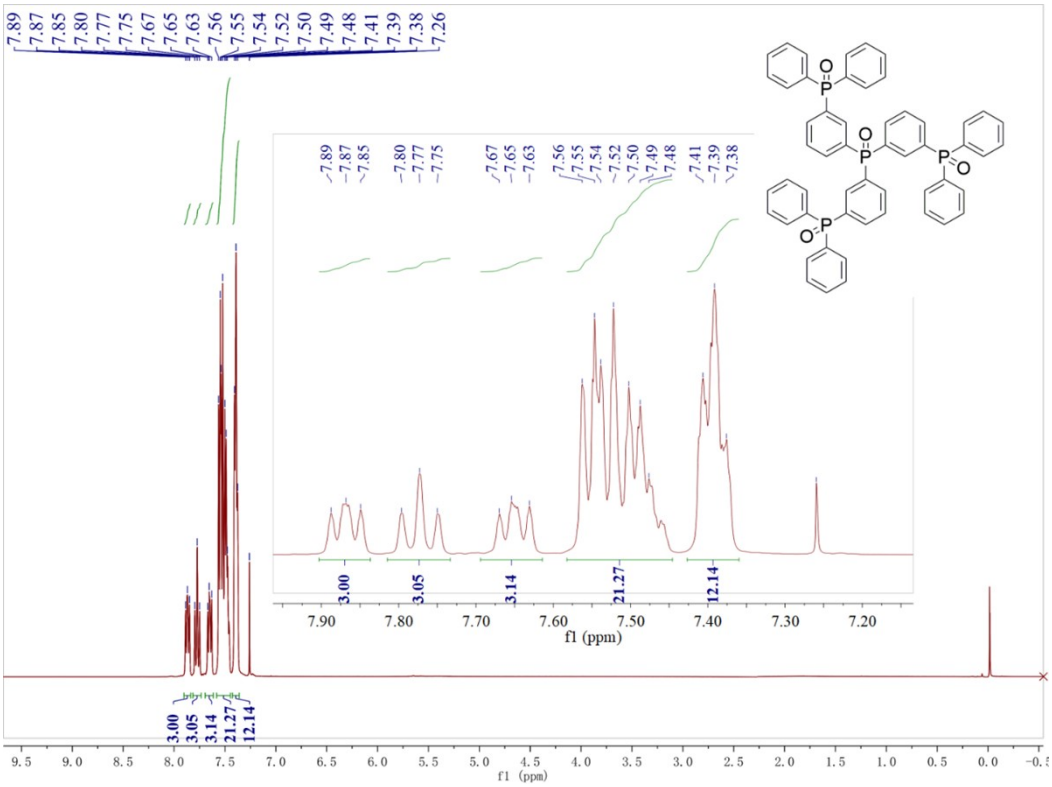

Figure S15. ^{1}H NMR spectra of **m4PO** in $CDCl_3$.

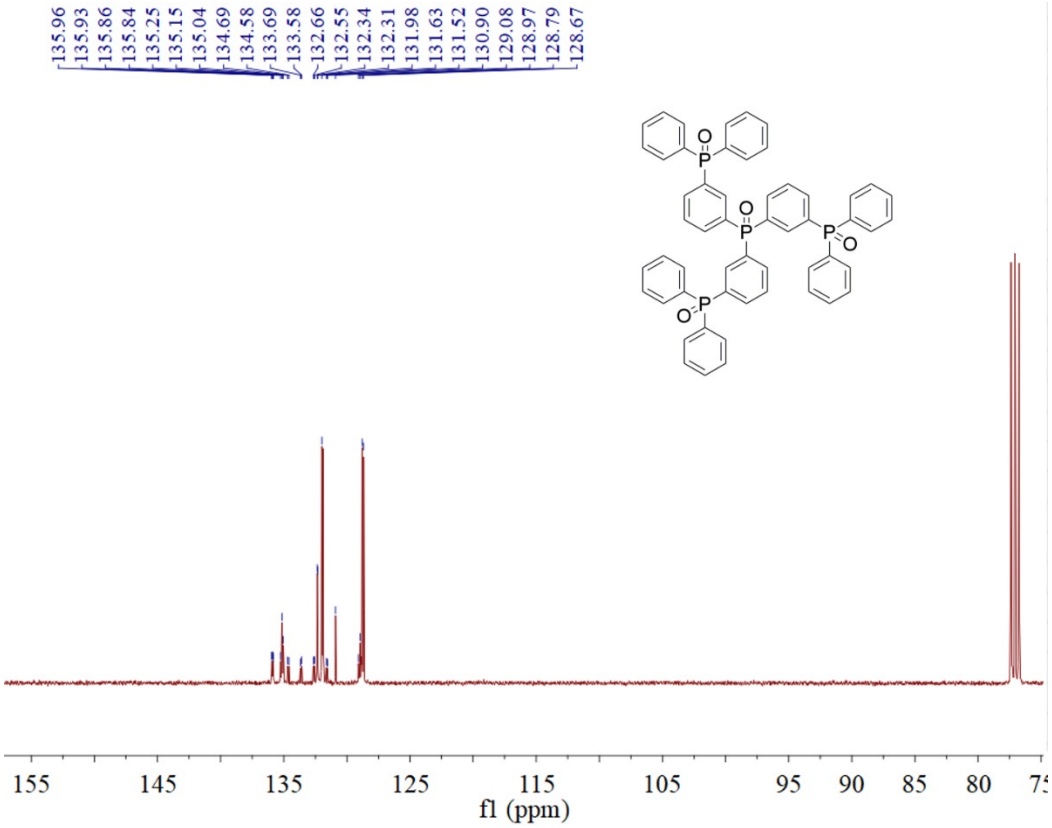

Figure S16. ^{13}C NMR spectra of **m4PO** in $CDCl_3$.

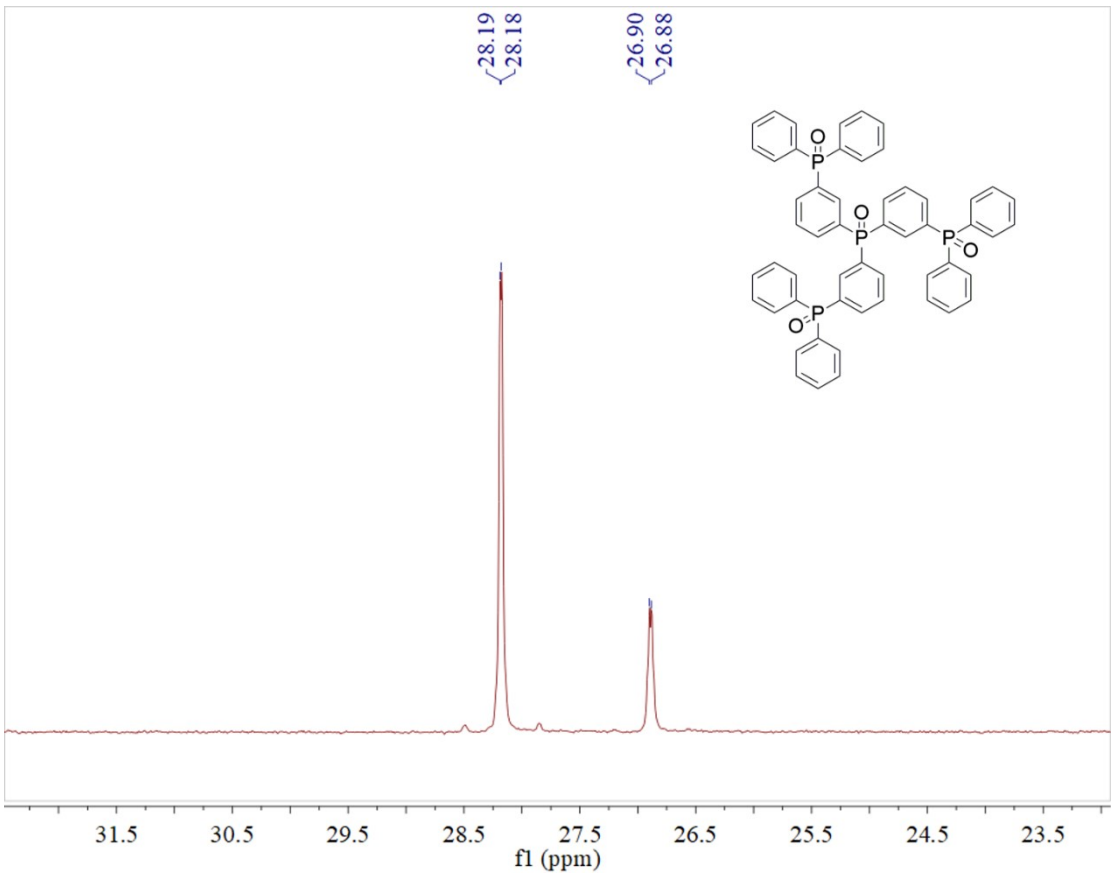

Figure S17. ^{31}P NMR spectra of **m4PO** in $CDCl_3$.

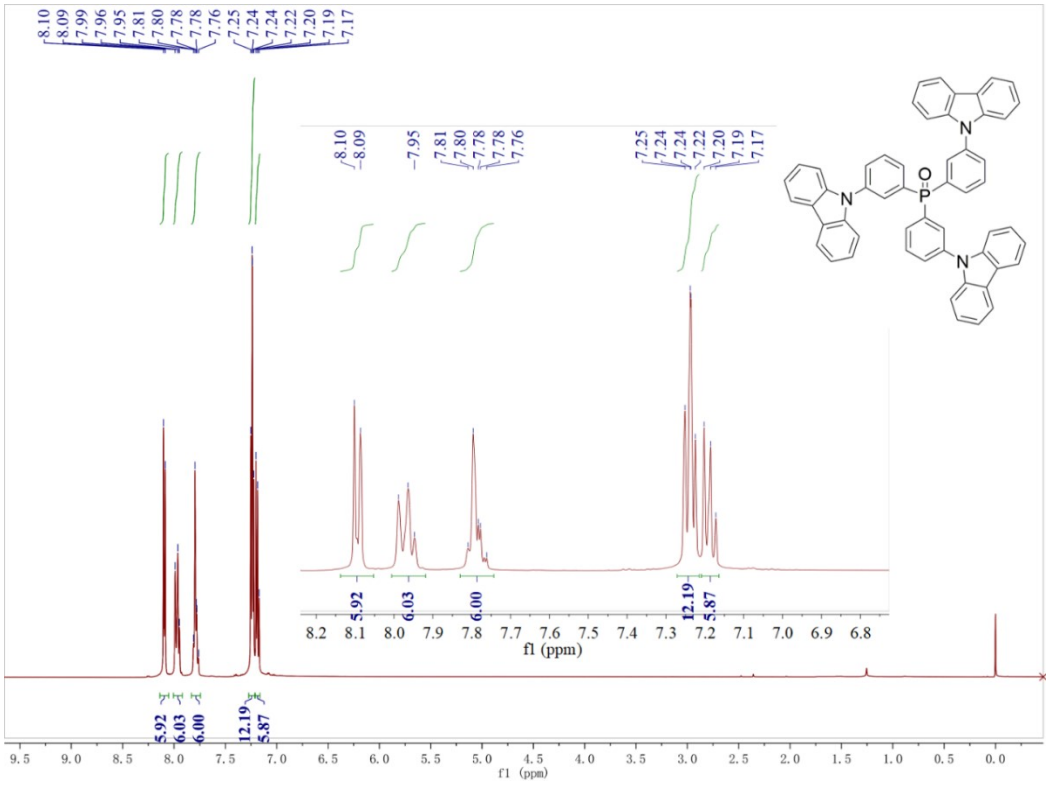

Figure S18. ^{1}H NMR spectra of **m3CzPO** in $CDCl_3$.

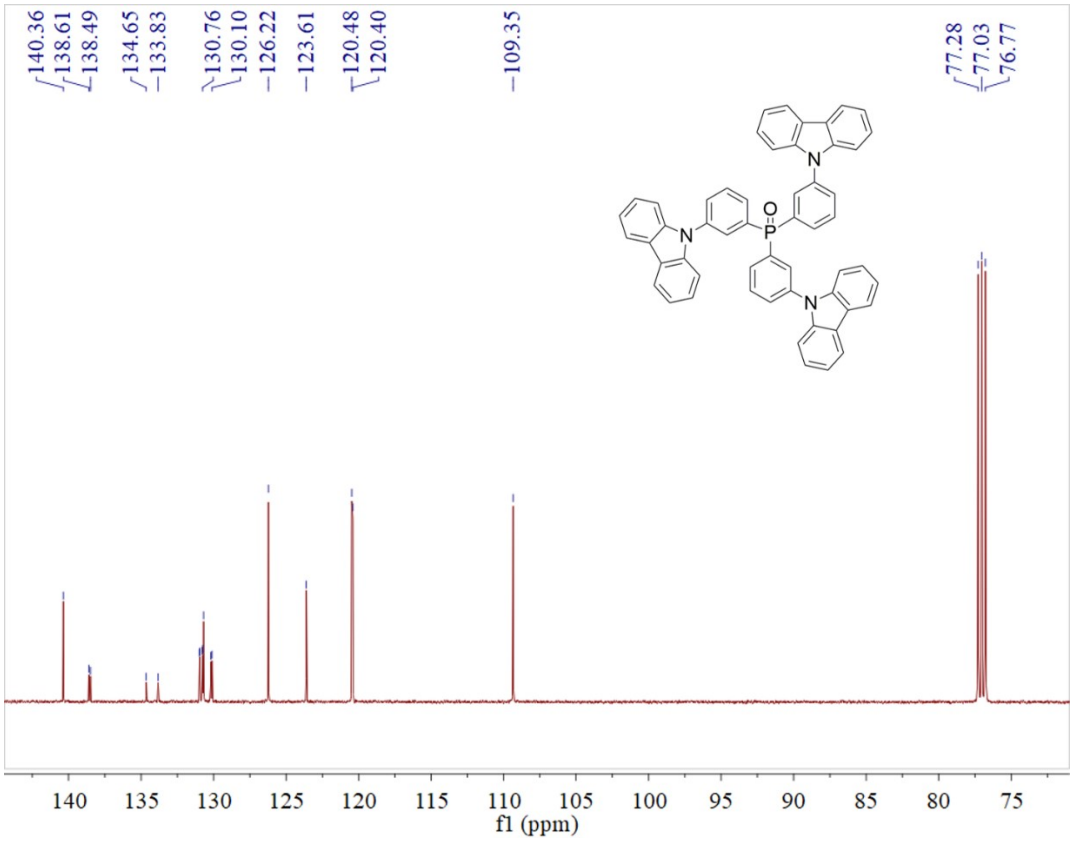

Figure S19. ^{13}C NMR spectra of **m3CzPO** in $CDCl_3$.

12. Mass spectra

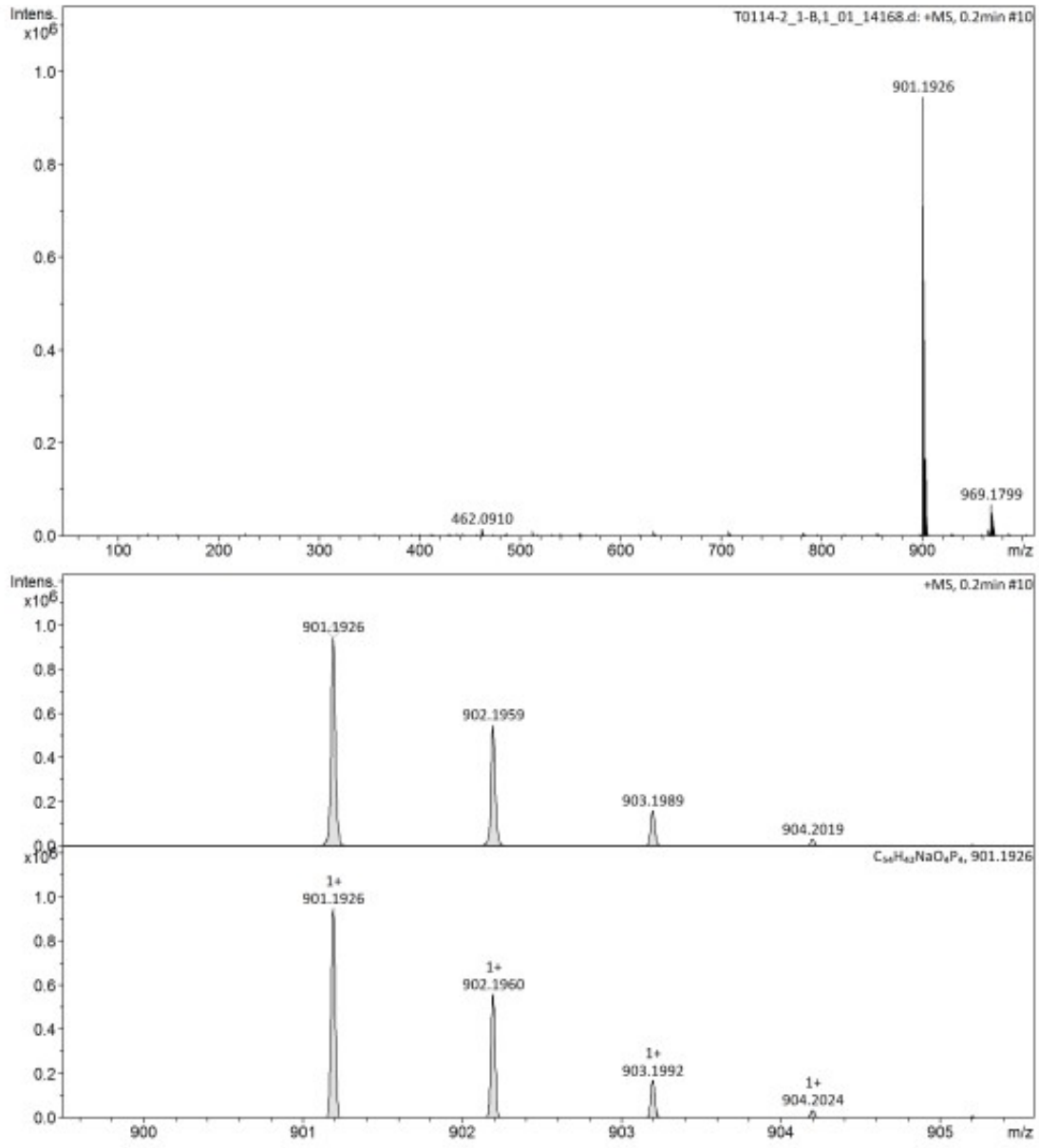

Figure S20. High resolution mass spectrometry of **m4PO**.

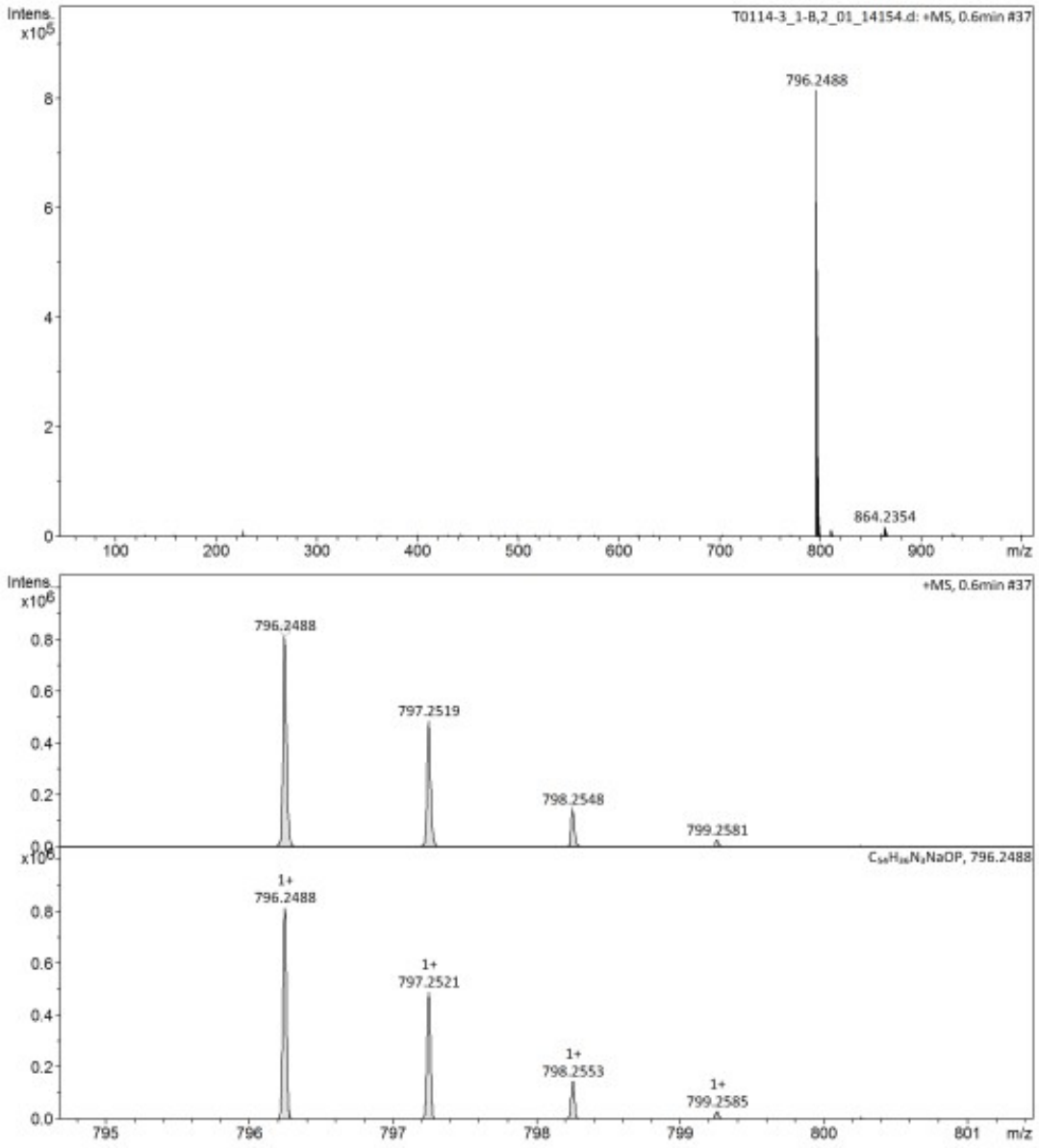

Figure S21. High resolution mass spectrometry of **m3CzPO**.

13. The comparison of hosts

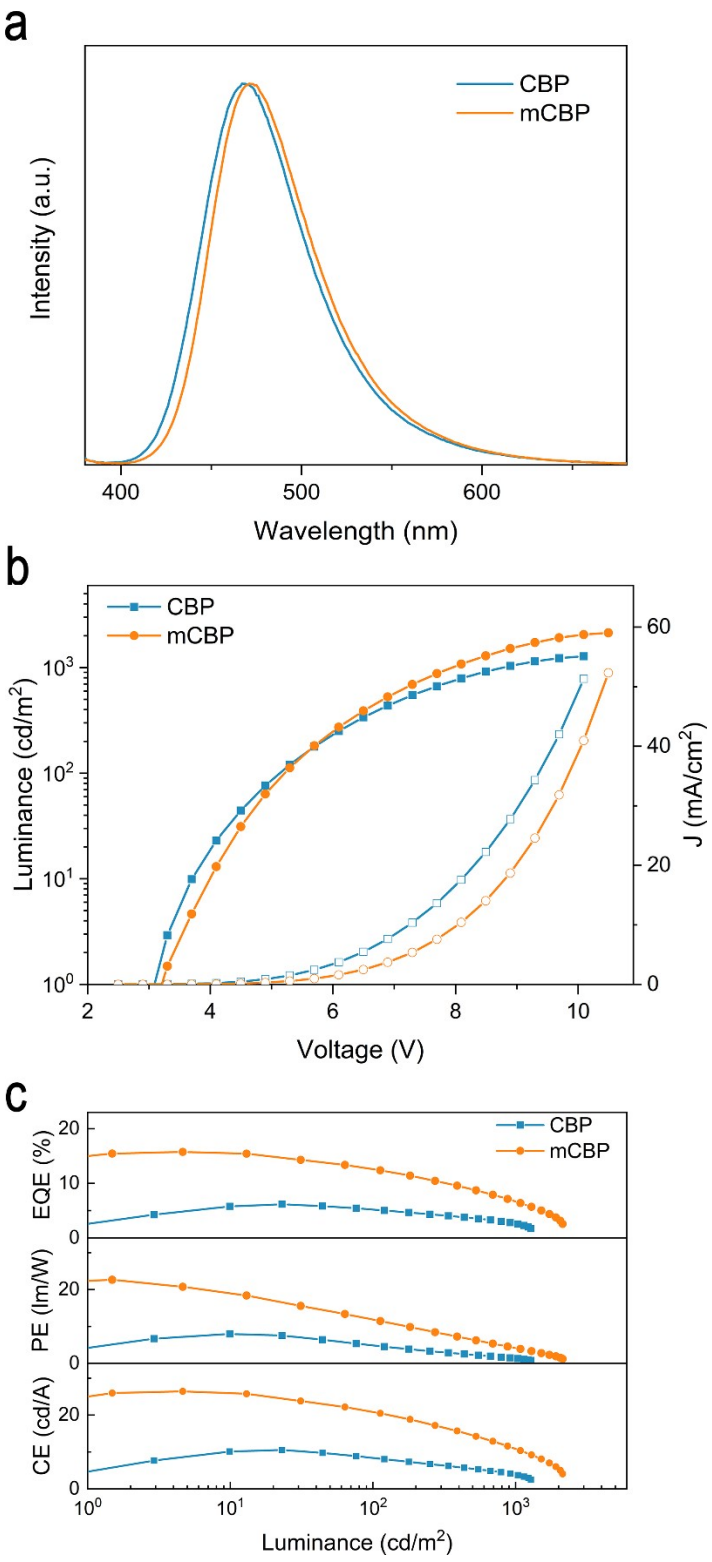

Figure S22. (a) Electroluminescence (EL) spectrum with the structure of ITO/MoO_3 (6 nm)/NPB (70 nm)/mCP (10 nm)/HOST: DMAC-DPS (30 wt%, 30 nm)/**m4PO** (10 nm)/BPhen (40 nm)/LiF (1 nm)/ Al (100 nm); (b) Current density-luminance-voltage (J-V-L) characteristics; (c) External quantum efficiency (EQE), power efficiency (PE) and current efficiency (CE) versus luminance characteristics.

Table S4. EL performance of blue TADF diodes.

Host	emitter	λ_{EL} [a] [nm]	L_{max} [b] [cd/m^2]	V [c] [V]	CE_{max} [cd/A]	PE_{max} [lm/W]	EQE_{max} [%]	CIE [d]
CBP	DMAC-DPS	467	1280	3.2	10.5	8.0	6.2	(0.15, 0.20)
mCBP	DMAC-DPS	471	2133	3.3	26.4	22.7	15.8	(0.16, 0.22)

[a] EL maximum wavelength at 6V; [b] The maximum luminance; [c] turn-on voltage taken at 1 cd/m^2; [d] value at 500 cd/m^2.

Table S5. EL performance of representative DMAC-DPS-based diodes

Host	L_{max} [b] [cd/m^2]	V [c] [V]	CE_{max} [cd/A]	PE_{max} [lm/W]	EQE_{max} [%]	CIE	Ref.
DPEPO	~10000	3.7	/	/	19.5	0.16, 0.20	[4]
24'DPEPO	~6500	3.5	30.6	27.5	20.1	0.16, 0.17	[5]
DBOSSPO	10588	3.0	28.5	29.8	19.0	0.16, 0.15	[6]
DPETPO	12747	2.8	39.7	44.4	23.0	0.16, 0.21	[7]
TPPO	1604	3.5	22.1	18.2	13.5	0.16, 0.19	[8]
DPDPO2A	14626	2.5	42.1	52.9	22.5	0.16, 0.23	[9]
BPOA2	27186	2.3	43.4	68.1	23.9	0.15, 0.23	[8]
9CzFDBFSPO	15928	3.0	28.2	29.6	16.7	0.17, 0.21	[10]
9CzFDBFDPO	15393	3.0	34.2	35.8	20.2	0.18, 0.22	[10]
9PhCzFDBFSPO	8124	3.0	21.3	22.3	13.4	0.16, 0.19	[10]
9PhCzFDBFDPO	7675	3.0	24.8	26.0	15.6	0.16, 0.20	[10]
9CzFSPO	~4000	3.5	21.4	19.2	12.2	0.16, 0.23	[11]
9CzFDPESPO	~6000	3.5	31.3	28.1	16.7	0.16, 0.23	[11]
9CzFDPEPO	~6000	3.5	25.1	22.4	13.2	0.16, 0.23	[11]
2,6-PFCzPy	1356	4.7	14.4	/	6.2	/	[12]
2,6-CzPy	6459	5.0	21.0	/	10.36	/	[12]
CzCbPy	8035	3.0	35.0	/	22.9	0.15, 0.26	[13]
2CzCbPy	6624	4.0	31.3	/	18.8	0.16, 0.28	[13]
PSAPO	10350	3.1	29.2	/	12.4	/	[14]
PSAPS	6926	2.9	32.0	/	13.8	/	[14]
DCzC	407	4.0	18.5	15.5	10.6	(0.16, 0.26)	[15]
DCzCO	5092	4.0	35.1	26.9	20.5	(0.16, 0.24)	[15]
SXDPO	14000	3.0	37.5	39.2	20.9	(0.16, 0.22)	[16]
tBCzPPOSPO	18305	3.0	60.7	63.5	21.1	(0.36, 0.44)	[17]
PPO2	5180	3.0	36.1	/	27.8	(0.15, 0.22)	[18]
3DCPO	6562	2.8	32.5	/	23.9	(0.15, 0.22)	[18]
DCzT	2233	2.9	25.5	27.3	12.0	/	[19]

14. References

[1] K. Duan, D. Wang, M. Yang, Z. Liu, C. Wang, T. Tsuboi, C. Deng, Q. Zhang, *ACS Appl. Mater. Interfaces* **2020**, 12, 30591.

[2] G. W. T. M. J. Frisch, H. B. Schlegel, G. E. Scuseria, M. A. Robb, J. R. Cheeseman, G. Scalmani, V. Barone, B. Mennucci, G. A. Petersson, H. Nakatsuji, M. Caricato, X. Li, H. P. Hratchian, A. F. Izmaylov, J. Bloino, G. Zheng, J. L. Sonnenberg, M. Hada, M. Ehara, K. Toyota, R. Fukuda, J. Hasegawa, M. Ishida, T. Nakajima, Y. Honda, O. Kitao, H. Nakai, T. Vreven, J. A. Montgomery Jr., J. E. Peralta, F. Ogliaro, M. Bearpark, J. J. Heyd, E. Brothers, K. N. Kudin, V. N. Staroverov, R. Kobayashi, J. Normand, K. Raghavachari, A. Rendell, J. C. Burant, S. S. Iyengar, J. Tomasi, M. Cossi, N. Rega, J. M. Millam, M. Klene, J. E. Knox, J. B. Cross, V. Bakken, C. Adamo, J. Jaramillo, R. Gomperts, R. E. Stratmann, O. Yazyev, A. J. Austin, R. Cammi, C. Pomelli, J. W. Ochterski, R. L. Martin, K. Morokuma, V. G. Zakrzewski, G. A. Voth, P. Salvador, J. J. Dannenberg, S. Dapprich, A. D. Daniels, Ö. Farkas, J. B. Foresman, J. V. Ortiz, J. Cioslowski and D. J. Fox, Gaussian 09, Revision D.01, Gaussian, Inc., Wallingford, CT, **2009**, 121, 150-166.

[3] F. W. C. T. C. Lu, Multiwfn: a multifunctional wavefunction analyzer, *J. Comput. Chem.*, **2012**, 33, 580.

[4] B. L. Q. Zhang, S. Huang, H. Nomura, H. Tanaka, C. Adachi, *Nat. Photon.* **2014**, 8, 326.

[5] D. D. J. Zhang, Y. Wei, H. Xu, *Chem. Sci.* **2016**, 7, 2870.

[6] D. D. J. Li, Y. Wei, J. Zhang, H. Xu, *Adv. Opt. Mater.* **2016**, 4, 522.

[7] J. Zhang, D. Ding, Y. Wei, F. Han, H. Xu, W. Huang, *Adv. Mater.* **2016**, 28, 479.

[8] F. Gao, R. Du, F. Jiao, G. Lu, J. Zhang, C. Han, H. Xu, *Adv. Opt. Mater.* **2020**, 8, 2000052.

[9] H. Yang, Q. Liang, C. Han, J. Zhang, H. Xu, *Adv. Mater.* **2017**, 29, 1700553.

[10] Z. Zhang, D. X. Ding, Y. Wei, J. Zhang, C. M. Han, H. Xu, *Chem. Eng. J.* **2020**, 382, 122485.

[11] D. X. Ding, Z. Zhang, Y. Wei, P. F. Yan, H. Xu, *J. Mater. Chem. C* **2015**, 3, 11385.

[12] C.-M. H. X.-H. Zhao, Y. Li, M.-G. Bai, J.-C. Yang, H. Xu,, L.-H. X. S.-D. Yuan, Z.-J. Xu, *Dyes Pigm.* **2020**, 175, 108127.

[13] D. H. A. J. S. Moon, S. W. Kim, S. Y. Lee, J. Y. Lee, J. H. Kwon, *RSC Adv.* **2018**, 8, 17025.

[14] X. H. Zhao, C. B. Duan, X. Ma, G. D. Zou, J. Zhang, H. Xu, L. H. Xie, S. D. Yuan, Y. J. Yang, W. Huang, *Org. Electron.* **2021**, 95, 106193.

[15] H. Jiang, Y. Tao, J. B. Jin, Y. Z. Dai, L. J. Xian, J. Wang, S. Wang, R. F. Chen, C. Zheng, W. Huang, *Mater. Horiz.* **2020**, 7, 3298.

[16] R. M. Du, C. B. Duan, Y. Li, J. Zhang, C. M. Han, H. Xu, *Chem. Eng. J.* **2020**, 392.

[17] C. M. Han, W. B. Yang, H. Xu, *Chem. Eng. J.* **2020**, 401.

[18] D. H. Ahn, J. S. Moon, S. W. Kim, S. Y. Lee, D. Karthik, J. Y. Lee, J. H. Kwon, *Org. Electron.* **2018**, 59, 39.

[19] H. H. Li, Y. Z. Wang, L. Yu, C. Liu, C. F. Zhou, S. B. Sun, M. G. Li, Y. Tao, G. Z. Xie, H. Xu, W. Huang, R. F. Chen, *Chem. Eng. J.* **2021**, 425.